Available online at www.sciencedirect.com
ScienceDirect
International Journal of Heat and Mass Transfer 50 (2007) 3062–3071
International Journal of HEAT and MASS TRANSFER
www.elsevier.com/locate/ijhmt

Effects of the pulsating flow agitation on the heat transfer in a triangular grooved channel

D.X. Jin, Y.P. Lee, D.-Y. Lee *

Thermal/Flow Control Research Center, Korea Institute of Science and Technology, Seoul 136-791, Republic of Korea

Received 12 May 2006; received in revised form 10 November 2006
Available online 21 February 2007

Abstract

Heat transfer enhancement by pulsating flow in a triangular grooved channel has been experimentally investigated for the ranges of $270 \leqslant Re \leqslant 910$ and $0.08 \leqslant St \leqslant 0.67$. It is measured that the heat transfer improved up to 350% at $Re = 270$ and $St = 0.34$ compared with the steady flow case. The heat transfer enhancement is found to increase as Reynolds number decreases. It is also found that the optimal Strouhal number increases as Reynolds number decreases. To analyze the correlation between the pulsating flow behaviors and the heat transfer enhancement characteristics, a PIV investigation has been performed. The PIV results show that the heat transfer enhancement results from the strong mixing caused by the repeating sequence of vortex generation, growth, expansion and ejection from the groove to the main stream by the pulsating flow. The fluid mixing enhancement is maximized when the pulsation period matches with the time duration for the vortex to grow large enough to fill the groove and then to be ejected to the main stream.

Keywords: Pulsating flow; Grooved channel; Heat transfer enhancement; PIV; Vortex; Fluid mixing

1. Introduction

This experimental study is to investigate the effects of pulsating flow field characteristics on the heat transfer enhancement in a triangular shape grooved channel. This work was motivated to inspect the possibility of heat transfer enhancement by the pulsating flow actuation in a flat plate heat exchanger. Similar research has been carried out by a number of researchers in a somewhat different geometry, rectangular shape grooved channel.

Ghaddar et al. [1] employed numerical simulation techniques to report the resonant heat transfer enhancement mechanism driven by pulsating flows. Greiner [2] reported the proving results for the same characteristics through experimental studies. He performed the experiments at Reynolds number of 700, pulsation fraction of 20%. In his experiment, heat transfer enhancement caused by the pulsating flow field resonance was monitored and the heat transfer enhancement of 160% at its optimum resonant frequency was reported. Mackley and Stonstreet [3] experimentally noticed the enhanced heat transfer in a baffled tube with pulsating flow agitation. Kim et al. [4] carried out a numerical study to investigate the heat transfer enhancement phenomena in case of pulsating channel flow where two heated blocks were used as a heat source. Based on the numerical results, they presented the existence of a resonance effect that the heat transfer enhancement is maximized under a certain frequency of pulsating flow. Recently, Moon et al. [5] verified experimentally the existence of the resonance of a pulsating flow in a channel with multiple rectangular blocks spaced periodically.

Nishimura et al. [6] performed extensive experimental study about mass transfer phenomena over a wide range of variables such as groove length, pulsation fraction, mean flow rate, and pulsation frequency. They reported the results of strong increase of mass transfer by the pulsating flow. Also, they showed the existence of optimum pulsation frequency where the enhancement of mass transfer is

* Corresponding author. Tel.: +82 2 958 5674; fax: +82 2 958 5689.
E-mail address: ldy@kist.re.kr (D.-Y. Lee).

0017-9310/$ - see front matter © 2007 Published by Elsevier Ltd.
doi:10.1016/j.ijheatmasstransfer.2006.12.001

Nomenclature

a	groove depth (m)
d	vortex diameter (m)
E	heat transfer enhancement ratio
f	pulsation frequency (Hz)
H	channel height (m)
h	heat transfer coefficient (W/m^2 K)
k	thermal conductivity (W/m K)
L	groove length (m)
$\dot{m}$	total flow rate (kg/s)
$\dot{m}_p$	pulsating flow rate (kg/s)
Nu	Nusselt number
q	heat flux (W/m^2)
Re	Reynolds number
St	Strouhal number
t	time (s)
T	pulsation period (s)
ΔT	temperature difference between the grooved wall and the fluid (K)
u	flow velocity at the smallest cross-section (m/s)
U	mean flow velocity at the smallest cross-section (m/s)
W	channel width (m)
x	ordering number of the groove

Greek symbols

η	pulsation fraction
ν	kinematic viscosity (m^2/s)
ω	angular velocity of vortex (rad/s)
Ω	dimensionless angular velocity of vortex

maximized. Nishimura and his colleagues [7,8] indicated that the active mixing between the main stream flow and the vortical flows within the wrinkled area created by the pulsating flow is the key mechanism for the mass transfer enhancement in the wrinkled channel. Within their experimental range, monotonic increase of mass transfer was noticed as the pulsation frequency increased. Also, Lee et al. [9] studied the effects of pulsating flow to the mass transfer in an axi-symmetrically wrinkled tube with numerical analysis. In their study, they showed that a specific pulsation frequency exists to obtain the maximum mass transfer.

As was mentioned, the present work was motivated to carefully inspect the possibility of heat transfer enhancement by the pulsating flow actuation in a flat plate heat exchanger. As a fundamental study, an experimental setup of a triangular shape grooved channel was designed, and a set of heat transfer enhancement experiments were performed. While the actual flow pattern in the flat plate heat exchanger is fully three dimensional and extremely complicated [10], the fundamental flow structure is a free stream flow over a plate with a sequence of triangular shaped grooves. In this research, while preserving the characteristics of the actual flow, a simplified model of the flow path was used for the experimental analysis.

A parametric study of multiple variables such as the pulsation frequency and Reynolds number is carried out and their effects on the heat transfer characteristics are analyzed. In addition, a PIV experiment has been performed for flow visualization and quantitative analysis of pulsating agitation of the flow field. Using the PIV results, the flow field is analyzed to show the timewise evolution of the vortex diameter, the vortex angular velocity, and the location of the vortex center. Lastly, the effect of the pulsation frequency on the flow field agitation is investigated to clarify the fundamental mechanism of the heat transfer enhancement by the pulsating flow.

2. Experimental apparatus and procedure

The present study considers the heat transfer enhancement in a triangular shape grooved channel as shown in Fig. 1. An experimental study on a similar geometry has been carried out by Greiner et al. [11] but without the pulsating agitation. They reported that the heat transfer in the grooved channel improves as compared with that in a flat channel when the groove geometry is compatible with the flow condition to encourage the intrinsic instability of the fluid flow.

Referring to Greiner et al. [11], the current geometry of the grooved channel is chosen to improve the heat transfer even in case of steady flow without pulsating agitation: the groove aspect ratio of $L/a = 2$ is used and the ratio between the groove length and the channel height of $L/H = 1.2$ is selected. The channel has a height (H) of 15 mm and a width of 187.5 mm. The channel is composed of 30 grooves arranged in the flow direction.

The schematic diagram of the experimental setup is shown in Fig. 2. In order to obtain a uniform velocity at the entrance of the grooved channel, a bell mouth type of the channel entrance was designed. Pyrex glass and acrylic plate are applied to both sides of the channel and to the bottom of the channel, respectively, for the visualization of the flow inside. Gold plated film heater was mounted on the groove surface in order to supply constant heat flux

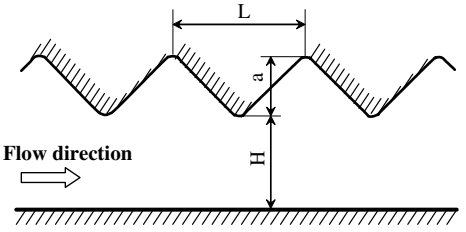

Fig. 1. Triangular shape grooved channel.

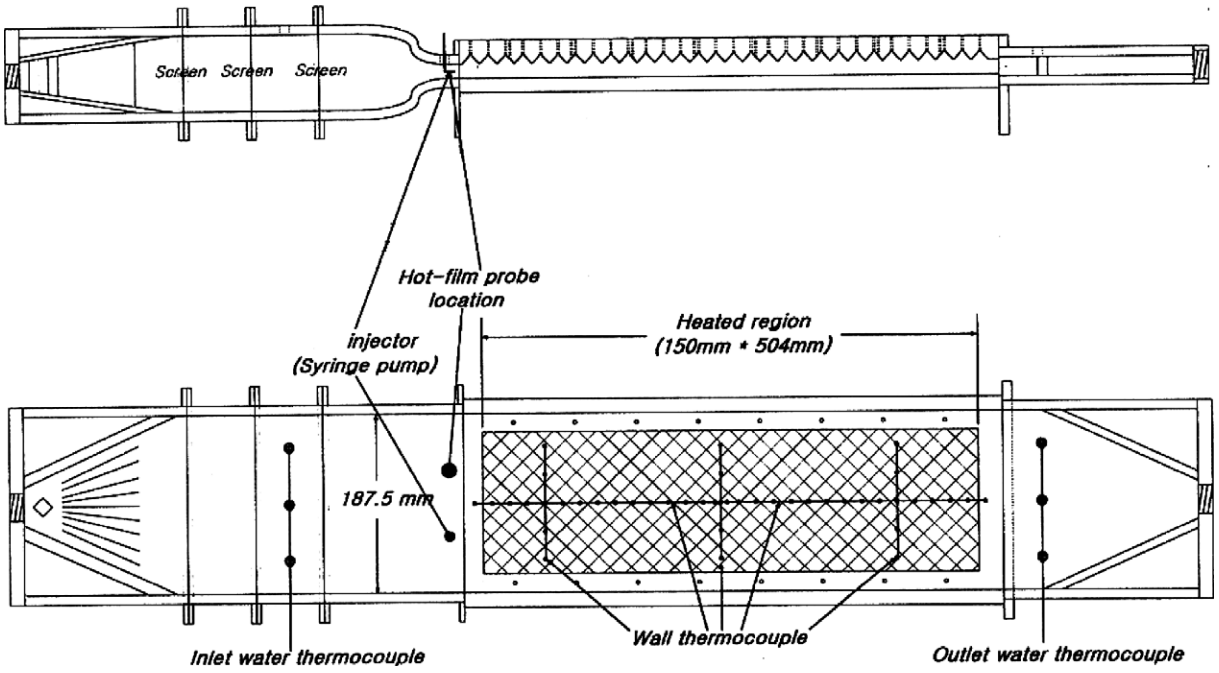

Fig. 2. Schematic diagram of the test section (water enters from the left).

from the triangular shaped groove surface to the fluid. The film heater was mounted from the 2nd groove to the 29th groove and was controlled by a power supply. In order to measure the temperatures of the fluid and the wall, a number of thermocouples were installed at various locations such as three at the entrance and three at the exit along the width of the channel for the fluid temperature measurement, and one at each of the groove valley for the wall temperature measurement. Additionally, to check the spanwise dependency of the heat transfer, four thermocouples were installed along the width of the groove at the groove valley at each of the front, middle and the rear parts of the channel.

The PIV system used in this study consists of a diode laser, a 480×420 resolution high-speed CCD camera and a computer that controls the PIV system. The tracer was polystyrene particles having a mean diameter of 45 μm. The velocity vector was obtained by a two frame cross-correlation PIV method. The interrogation window was set to be 32×32 pixels with 50% overlap.

Water was supplied to the channel using a centrifugal pump and a diaphragm pump with a specified flow rate, pulsation fraction, and frequency. Feed water was stored in a constant temperature reservoir (250 l) that was temperature-controlled with a 3 RT refrigerator. After water passed the test section, the flow rate was measured with a high accuracy electric scale and a stopwatch and then the water was returned back to the low temperature reservoir. Average temperature of the water at the test section was set at 21 ± 0.5 °C using a constant temperature reservoir, and the temperature difference between the wall and the water was controlled to be 5–10 °C by adjusting the heat supply. Pulsating flow rate (time averaged volume flow rate from the diaphragm pump) and frequency were controlled by adjusting the stroke and rotational speed of the diaphragm pump. The pulsating flow from the diaphragm pump and the steady flow from the centrifugal pump were merged just before the entrance and fed to the test section. The pulsation fraction is defined as the ratio of the pulsating flow rate from the diaphragm pump to the total flow rate:

$$\eta = \frac{\dot{m}_{\mathrm{p}}}{\dot{m}}. \tag{1}$$

In this work, the pulsation fraction was fixed at 0.5.

Reynolds number and Strouhal number are defined as

$$Re = \frac{UH}{v}, \tag{2}$$

$$St = \frac{fH}{U}, \tag{3}$$

where U is the mean flow velocity at the smallest cross-section of the channel.

After the average flow rate, pulsation fraction and frequency were set, heat was supplied by adjusting the power transformer. Once the wall temperatures reached the steady state, the temperature and the flow rate were measured. Using the measured values of wall temperature, mixed mean water temperature and heat flux, the local average Nusselt numbers at the places of thermocouples were obtained as

$$\overline{Nu}_{2\to x} = \frac{\bar{h}_{2\to x} H}{k}, \tag{4}$$

$$\bar{h}_{2\to x} = \frac{(x-1)q}{\sum_{i=2}^{x} \Delta T_i} \tag{5}$$

where q is the heat flux from the grooved wall, x the ordering number of the groove, and ΔT_i is the local temperature difference between the wall and the bulk fluid at each groove.

The heat transfer enhancement ratio is evaluated as

$$E = \frac{\overline{Nu}_{2\to 29}}{\overline{Nu}_{2\to 29,\eta=0}}. \quad (6)$$

3. Heat transfer enhancement

3.1. Steady flow case ($\eta = 0$)

In order to evaluate the characteristics of heat transfer enhancement by the pulsating flow, cases for the steady flow were tested out for comparison. The local average Nusselt numbers for the steady flow cases are presented in Fig. 3. For the cases of $Re = 270$ and 370, laminar flow patterns (no flow disruption) were observed from visual inspection over the whole length of the test section. In these cases, the local average Nusselt number decreases as the flow reaches the downstream of the channel. For the cases of $Re = 550$, 730, 910, the Tollmien–Schlichting waves [1,12] were observed to develop due to the instability of the boundary layer and transitions to turbulent flows were monitored at further downstream of the channel. It was also noticed that the location of the transition moved to upstream as Reynolds number increased. The locations of the flow transition are depicted in Fig. 3 as thick arrows. These locations are found to coincide well with the points where the local average Nusselt numbers starts to increase in each case. The Nusselt numbers obtained in this research matches well with the results ($4 < Nu < 13$) reported by Russ and Beer [13] for the case of wrinkled tube experiment. Furthermore, the locations where the Tollmien–Schlichting wave starts to develop are agreed reasonably well with the results obtained by Greiner et al. [11].

3.2. Pulsating flow case

In order to evaluate the effects of pulsating flow on the heat transfer enhancement through direct comparison with the steady flow case, the experiments were designed and carried out for the same Reynolds number based on the average flow rate. Various cases of pulsation frequency and Reynolds number were experimented and their results for $Re = 730$, $\eta = 0.5$ were presented in Fig. 4. As shown in Fig. 4, it is obvious that the local average Nusselt numbers are clearly increased by the pulsating flow. The enhancement effect is found dependent on the non-dimensional pulsation frequency, St. Up to 120% of heat transfer enhancement is achieved at some location while 75% of overall average is obtained over the whole channel length.

In Fig. 5, heat transfer enhancement ratios versus pulsation frequency are presented for various cases of Reynolds numbers. It is noticed that the heat transfer enhancement ratio decreases as Reynolds number increases.

Particularly, when the pulsation frequency is low, the heat transfer enhancement ratio increases with increasing the pulsation frequency. However, once the heat transfer enhancement ratio reaches its maximum value at a certain frequency, it starts to decrease as the pulsation frequency continues to increase. This phenomenon clearly illustrates the existence of the optimum frequency for the maximum heat transfer enhancement ratio. The optimum Strouhal number is shown to decrease as Reynolds number increases. These results show the same trends obtained by the previous numerical calculation from Lee et al. [9].

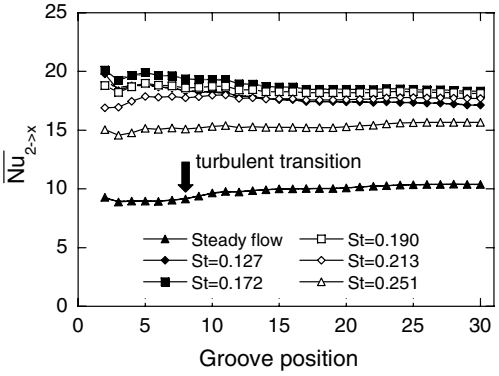

Fig. 4. Local averaged Nusselt number in pulsatile flow: $Re = 730$ and $\eta = 0.5$.

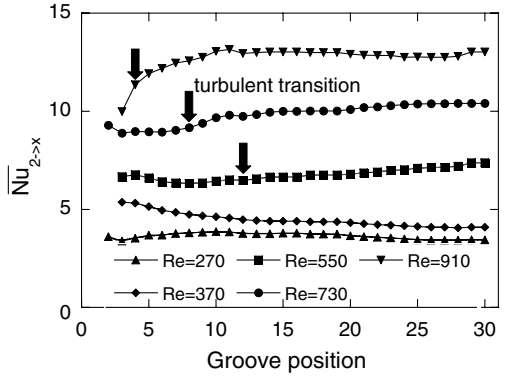

Fig. 3. Local averaged Nusselt number in steady flow.

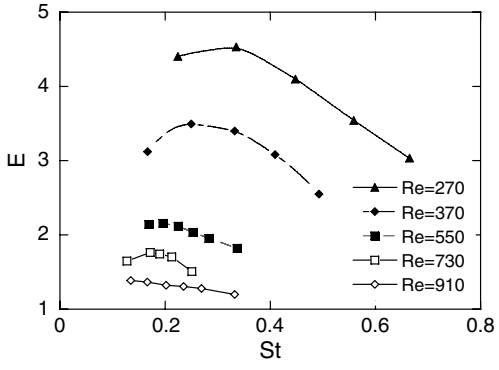

Fig. 5. Heat transfer enhancement ratio: $\eta = 0.5$.

It is also worthy to note the work of Greiner et al. [14] that the pulsating agitation necessitates only minor increase in the pumping power in low Reynolds number flow cases. Therefore, considering the heat transfer enhancement results shown in Fig. 5, the pulsating agitation appears to be very effective method of improving heat transfer at least in low Reynolds number applications.

4. Mechanism for the enhancement

4.1. PIV results

In order to clarify the fundamental mechanism of heat transfer enhancement by the pulsating flow, flow visualization and PIV experiments were performed with various pulsation frequencies at the condition of $Re = 370$ and $\eta = 0.5$. The PIV images were taken at the 12th groove. Preliminary test showed that the pulsating flow becomes fully developed from the 7th groove so that the velocity field repeats itself from groove to groove afterward.

Fig. 6 displays the visualization result for the comparison case of steady flow obtained by overlapping five successive images taken in the interval of 1/250 s. Flow direction is from the left to the right. A steady vortex is found rotating inside the groove and the main stream outside the groove appears hardly affected by the recirculating flow. In this case, it can be inferred that the mixing is not effective between the fluid inside the groove and the fluid in the main stream.

Fig. 7 shows the timewise variation of the cross-section averaged pulsating velocity at the location of the minimum channel cross-section in case of $Re = 370$, $St = 0.25$, and $\eta = 0.5$. The velocity is obtained by integrating, from the bottom to the top of the channel, the velocity vectors from the PIV analysis to yield the instantaneous flow rate at each channel cross-section and averaging them over the flow direction. In this study, the beginning point of a pulsation

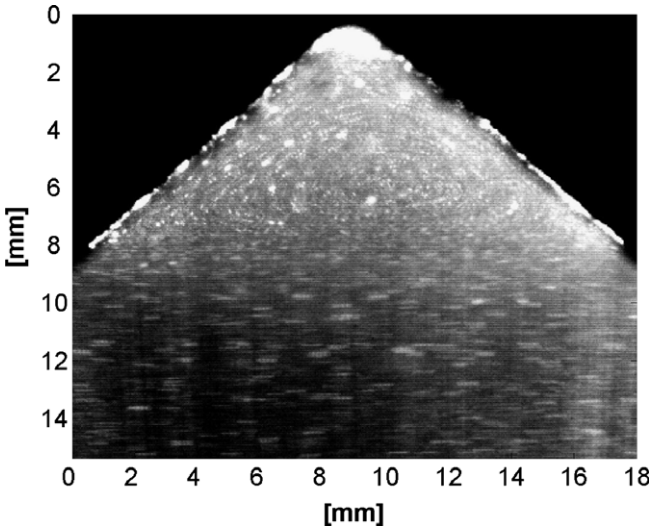

Fig. 6. Flow visualization for steady flow: $Re = 370$.

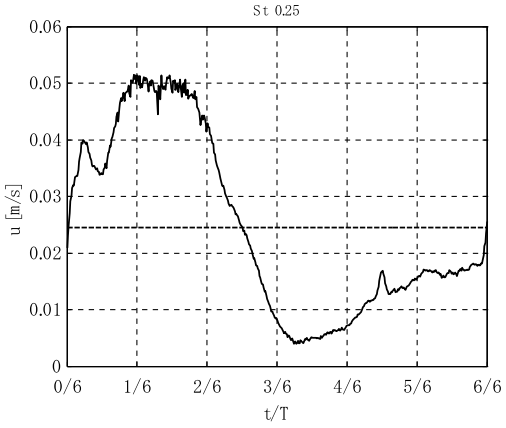

Fig. 7. Pulsating flow velocity: $Re = 370$, $St = 0.25$ and $\eta = 0.5$.

cycle is set to the point where the flow velocity reaches the mean velocity, U, during the acceleration phase.

Fig. 8 displays the flow visualization results for the case of $Re = 370$, $St = 0.25$ and $\eta = 0.5$. A sequence of six images, each of which is obtained by overlapping five successive images, shows the evolution of the velocity field within a single period of the flow pulsation. As the velocity of the channel flow increases ($t/T = 0/6, 1/6$), a vortex is generated at the tip of the groove. Once generated, the vortex travels along the free stream, collides to the other side of the groove wall and then rotates in the groove promoting the mixing of the fluid therein ($t/T = 2/6$). After that, as the main stream decelerates ($t/T = 3/6$), the vortex begins to entrain fluid from the relatively slow moving main stream and to grow gradually in size. As the influx of the slow moving fluid increases, the vortex is enlarged bigger than the size of the groove ($t/T = 4/6$) and eventually comes out to the main stream channel. Finally, this fully grown vortex is pulled by the main stream and ejected carrying the high temperature fluid from the groove ($t/T = 5/6$). As a result, mixing process between the vortex from the groove and the main stream is enhanced and eventually the heat transfer enhancement is achieved over the consecutive cycles.

Fig. 9 presents the instantaneous velocity fields obtained from PIV analysis. At $St = 0.17$, the overall process of the vortex generation, growth, and expansion is similar to that at $St = 0.25$. It is noteworthy, however, that the vortex is already leaving the groove when $t/T = 4/6$ in case of $St = 0.17$, while the vortex stays longer within the groove until $t/T = 5/6$ in case of $St = 0.25$. At $St = 0.42$, a vortex generated during the acceleration phase does not enter the groove but floats directly to the downstream ($t/T = 2/6$), and another vortex generated in the upstream groove floats into the groove right after and breaks up when the flow decelerates resulting in a very complex flow field.

4.2. Mixing enhancement

Since the PIV provides not only the flow patterns but also the detailed velocity measure, it enables a quantitative

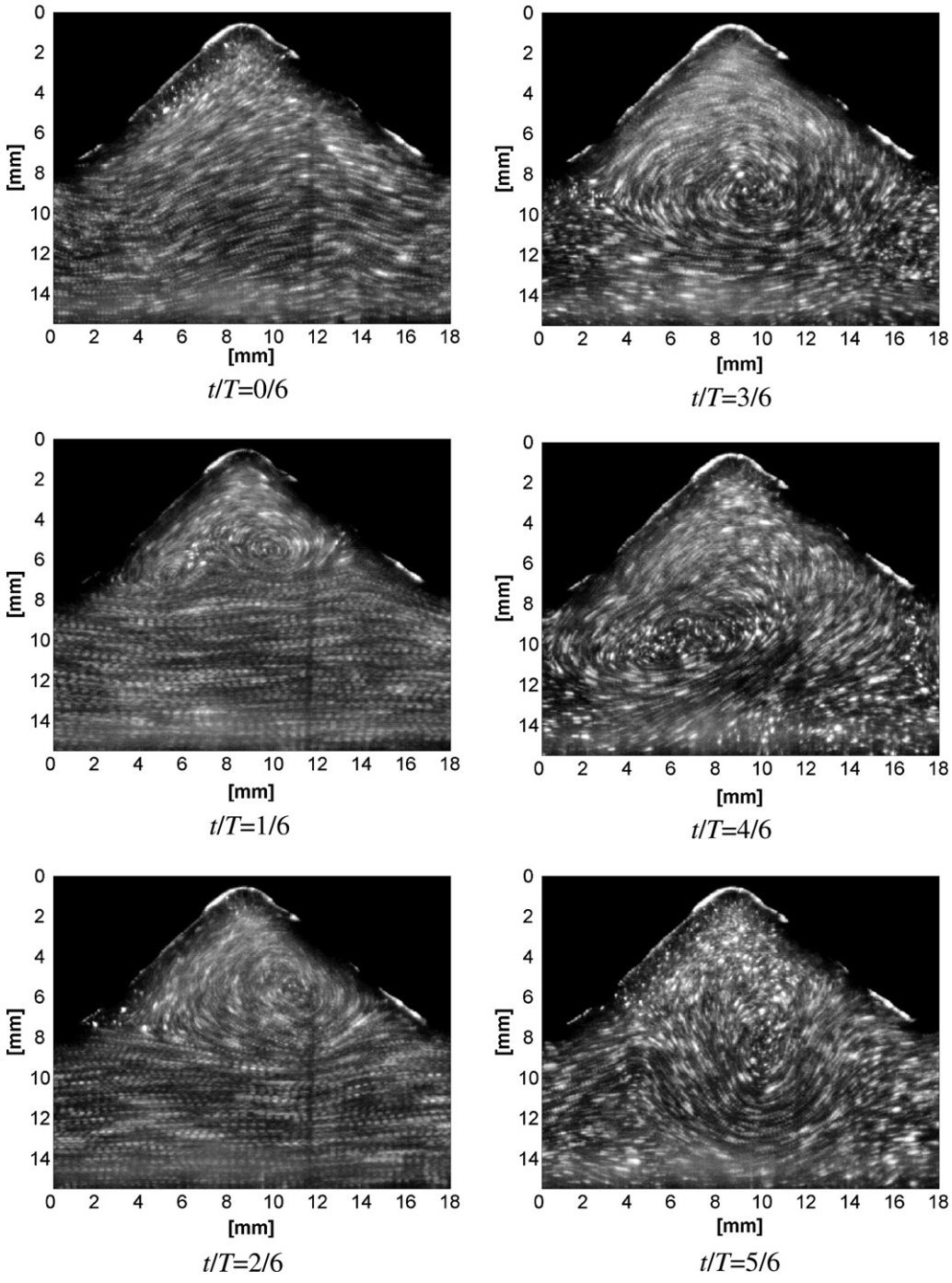

Fig. 8. Flow visualization: $Re = 370$, $St = 0.25$ and $\eta = 0.5$.

analysis on the pulsating agitation effect on the flow field. In this work, the stream function and the vorticity were evaluated at each time step from the instantaneous velocity field. Then, the streamlines were plotted for each time step and the vortex diameter was calculated from the area corresponding to the largest closed streamline. The angular velocity (ω) of the vortex was obtained from the average vorticity of the vortex and expressed in a dimensionless form as

$$\Omega = \frac{\omega H}{U}. \tag{7}$$

Figs. 10–12 display time evolutions of the diameter (d/H) and the angular velocity of the vortex ($\omega H/U$), and the trace of the vortex center, respectively. The vortex center is determined as the point where the vorticity has the maximum value. Since the moving velocity of the vortex center becomes nearly the same as the relative velocity at

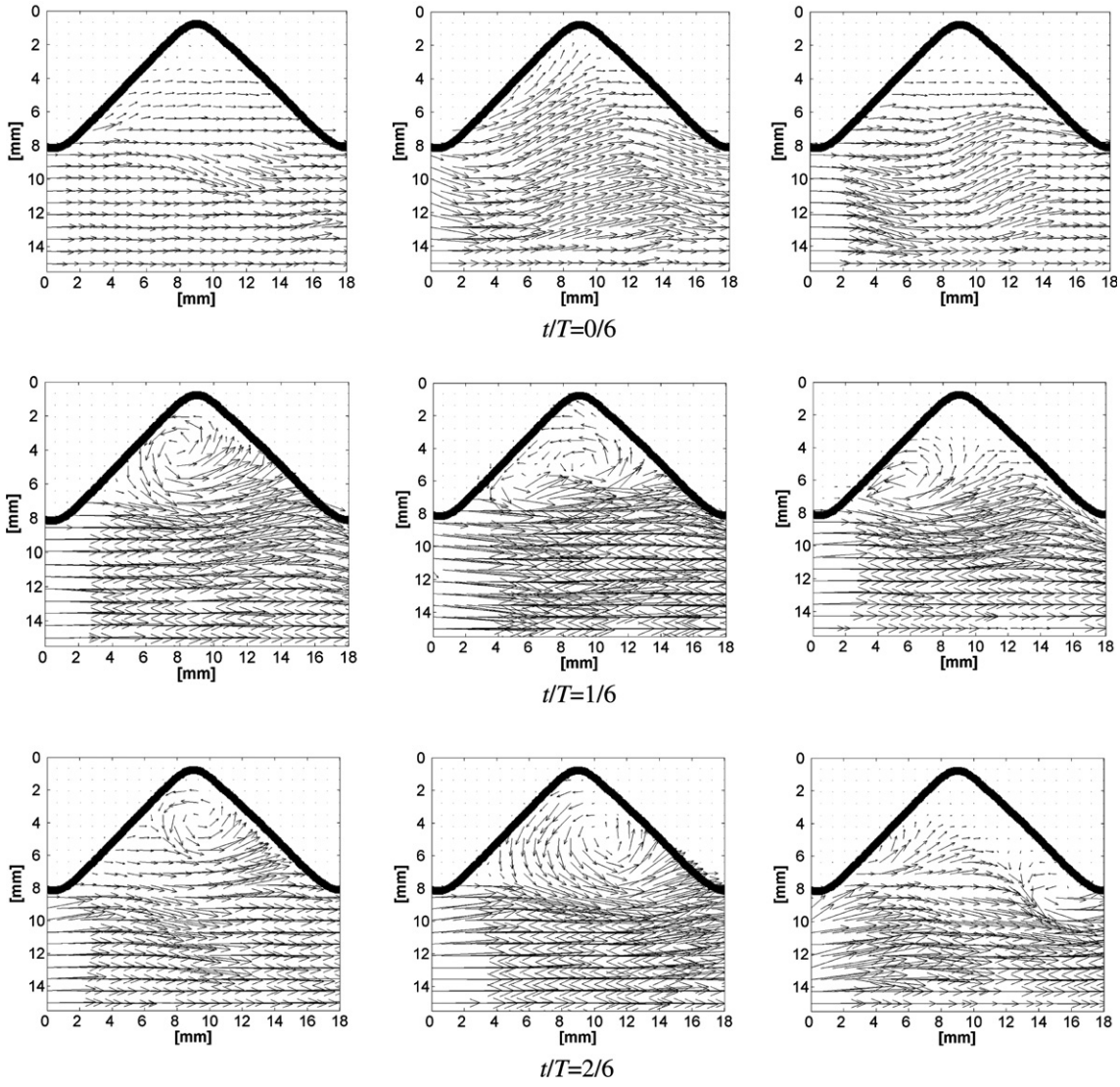

Fig. 9. Instantaneous velocity fields: $Re = 370$ and $\eta = 0.5$.

the vortex edge compared to the vortex center when the vortex is moving out of the groove, the vortex shape obtained apparently from the instantaneous streamline is considerably distorted as compared with that evident from the visual analysis of consecutive evolution of the flow field. In this reason in Fig. 10 the dimensionless diameter of the vortex is presented only up to the moment when the vortex is about to flow out of the groove.

When $St = 0.17$ and $St = 0.25$, as shown in Fig. 12a and b, the vortex center remains inside the groove during the acceleration phase of the main stream. Both the diameter and the angular velocity of the vortex grow rapidly at the beginning of the acceleration phase and then keep almost unchanged once the vortex fills the groove until the main stream begins to decelerate. When the main stream begins to decelerate, the vortex expands and grows bigger, whereas the vortex angular velocity decreases (see Figs. 10 and 11). Subsequently, as shown in Fig. 12, the vortex center comes out of the groove and finally floats to the downstream. The maximum values of the vortex diameter and vortex angular velocity before leaving the groove are almost the same in the two cases of $St = 0.17$ and $St = 0.25$. Meanwhile, at $St = 0.42$, the vortex (vortex 1 in Figs. 10–12) generated during the acceleration phase does not enter the groove but drifts downstream even before the vortex is fully grown. Then another vortex (vortex 2) floats from the upstream but is not grown either enough to affect the flow mixing inside the groove before broken into several small vortices.

Fig. 13 is a replot of Fig. 10 displaying the variation of the vortex diameter in a real time base. When $St = 0.17$ and $St = 0.25$, it is shown that the time duration for the vortex growth in the acceleration phase and that for the vortex expansion in the deceleration phase are almost the same between these two cases. This is because the growth or the expansion of the vortex is caused by the diffusion of

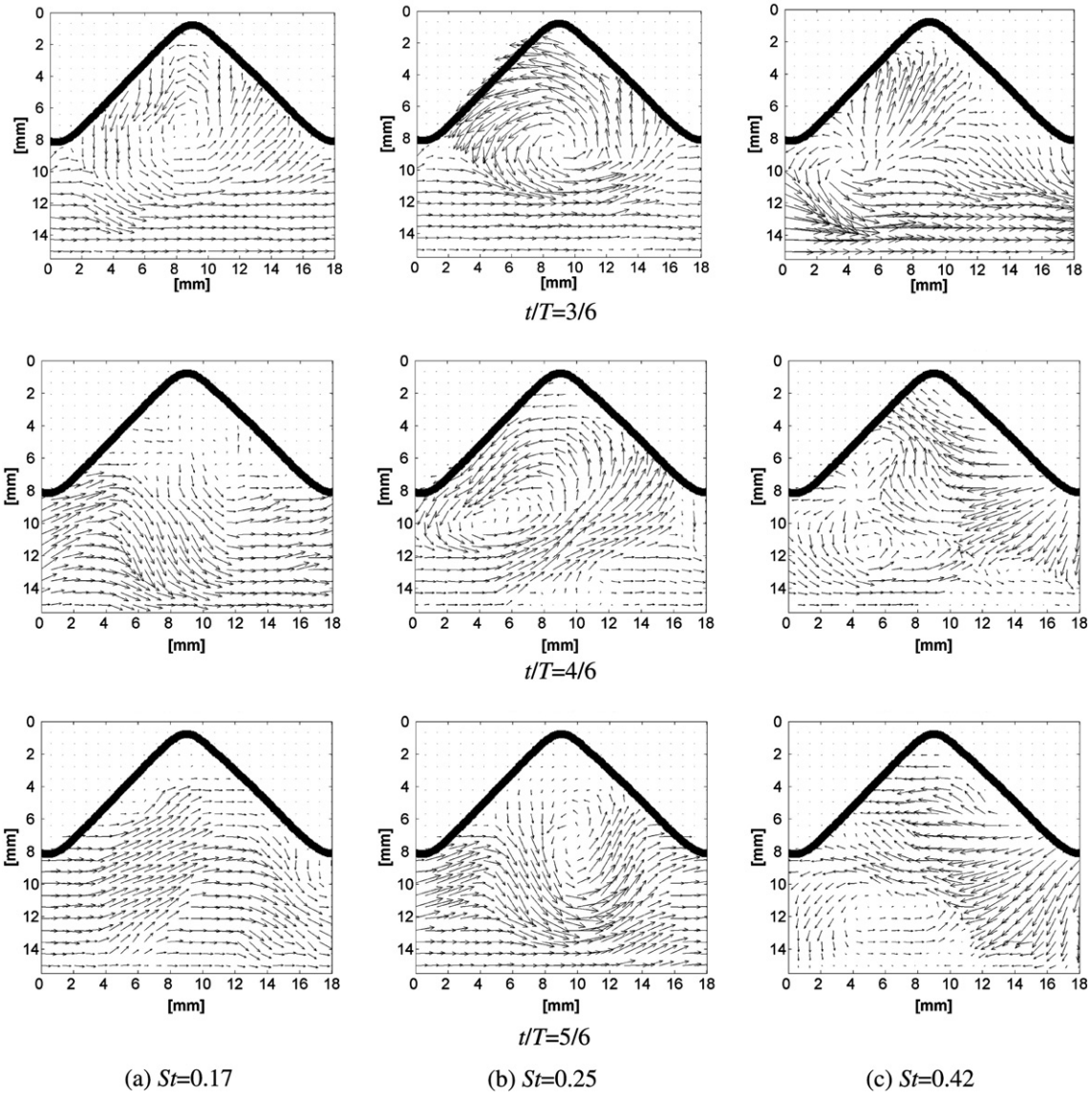

Fig. 9 (*continued*)

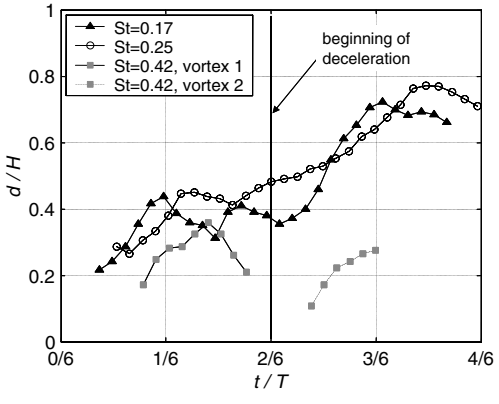

Fig. 10. Vortex diameter: $Re = 370$ and $\eta = 0.5$.

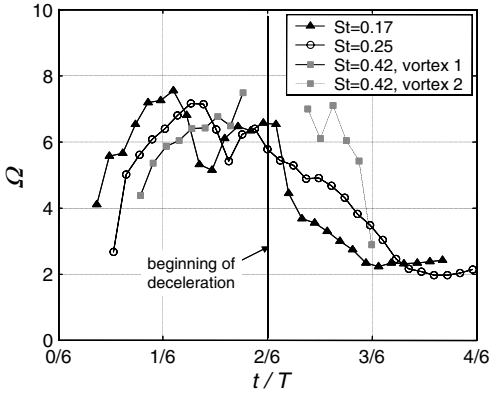

Fig. 11. Angular velocity of the vortex: $Re = 370$ and $\eta = 0.5$.

the shear layer between the two fluids having different velocities. Consequently, the growth or the expansion of the vortex takes a certain time dominated by the momentum diffusivity, which is obviously constant independent

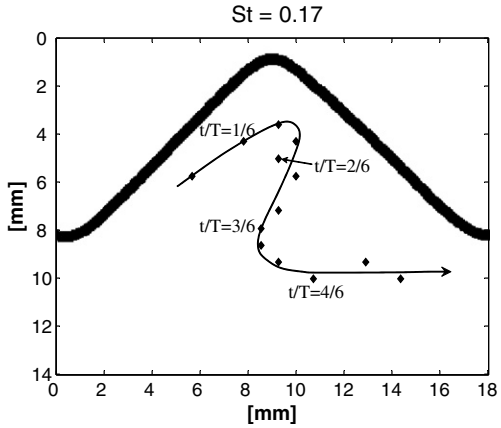

(a) *St*=0.17

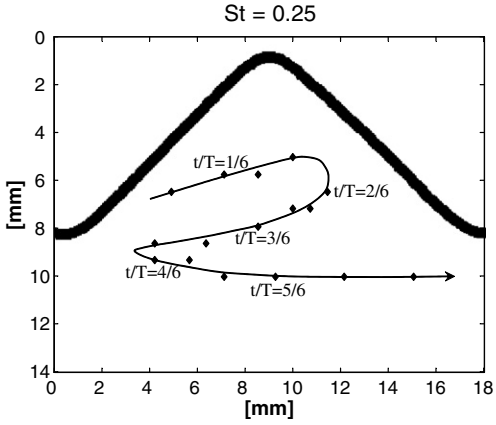

(b) *St*=0.25

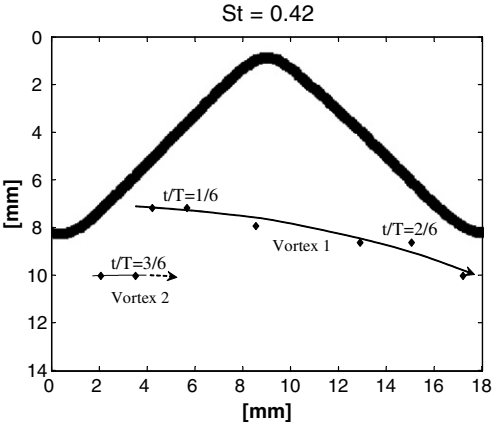

(c) *St*=0.42

Fig. 12. Trace of the vortex center: $Re = 370$ and $\eta = 0.5$.

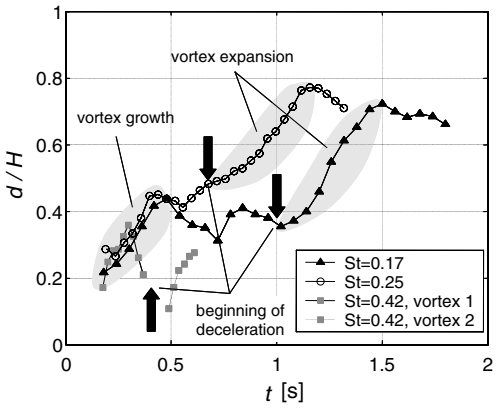

Fig. 13. Variation of the vortex diameter: $Re = 370$ and $\eta = 0.5$.

of the pulsation frequency. For the two cases of $St = 0.17$ and $St = 0.25$, the pulsation period is shown long enough for the vortex to grow and to expand to its full size, whereas the time period is too short in case of $St = 0.42$.

Meanwhile, at $St = 0.17$, the time intervals between the flow acceleration and deceleration are longer than those at $St = 0.25$. Therefore, the duration of the vortex maintaining almost the same size after growing large already enough to fill the groove in the acceleration phase or the duration of the interval from the vortex ejection to the beginning of the next acceleration is longer in the case of $St = 0.17$ as compared with the case of $St = 0.25$. In other words, the vortex ejection frequency is lower in the case of $St = 0.17$ than in the case of $St = 0.25$.

Considering the two aspects of the vortex growth and the vortex ejection, it is natural to anticipate the existence of the optimum pulsation frequency for the maximum heat transfer. When the pulsation frequency is too high, the vortex growth does not complete to satisfaction and the vortex expansion is not enough either for an effective ejection. On the contrary, if the pulsation frequency is too low, the number of ejection process for a given time is too low. Consequently, the heat transfer enhancement ratio is lower in either case than the one at the optimum pulsation frequency. With the optimum pulsation frequency, the pulsation period of the flow should be long enough for but not much longer than the vortex growth and expansion to its full size.

4.3. Effects of the Reynolds number

In the steady flow, the mixing process between the fluid in the main steam and the fluid inside the groove is promoted by self induced fluctuation due to the instability of the flow as the Reynolds number increases. Meanwhile in the pulsating flow, the fluid mixing is additionally promoted by the repeating sequence of vortex generation, growth, expansion, and then ejection from the groove to the main stream by the pulsating flow. As a consequence, the heat transfer from the wall to the main stream fluid is enhanced. As the Reynolds number becomes larger, the portion of the fluid mixing caused by the pulsating flow becomes smaller in the total fluid mixing effect because the fluid mixing caused by the self induced fluctuation becomes larger. Therefore, the heat transfer enhancement ratio of pulsating flow decreases as Reynolds number increases as shown in Fig. 5.

As the Reynolds number increases, the optimum Strouhal number decreases as shown in Fig. 5. This trend can be

understood as follows. As was noticed in the previous section, the time duration for the vortex growth and the vortex expansion is controlled by the momentum diffusivity. Therefore, the optimum pulsation frequency is relatively constant regardless of the free stream velocity. Consequently, the optimum Strouhal number decreases adversely proportional to the velocity as the Reynolds number increases.

5. Conclusions

This research was performed to verify the heat transfer enhancement effect of the pulsating flow agitation and to investigate the mechanism of the heat transfer enhancement by the pulsating flow agitation in a triangular shaped groove channel. Through extensive experiments and analyses following conclusions were derived.

(1) Pulsating flow agitation promotes the heat transfer. In the range of the present experimental study, a maximum of 350% of heat transfer enhancement is achieved compared to the steady flow case at $Re = 270$, $St = 0.34$, and $\eta = 0.5$.
(2) As the Reynolds number increases, the heat transfer enhancement ratio decreases.
(3) The existence of the optimum pulsation frequency for the maximum heat transfer enhancement is confirmed. When the Reynolds number increases, the optimum Strouhal number decreases.
(4) The repeating sequence of vortex generation, growth, expansion, and ejection from the groove to the main stream by the pulsating flow promotes strong mixing between the fluid inside the groove and the fluid in the main stream. As a consequence, the heat transfer is enhanced from the wall to the main stream fluid.
(5) The fluid mixing enhancement is maximized when the pulsation period matches with the time duration for the vortex to grow large enough to fill the groove and to be ejected to the main stream.
(6) Since the process of vortex growth and expansion is controlled by the momentum diffusivity, the optimum frequency is nearly constant regardless of the Reynolds number. Therefore, the optimum Strouhal number appears adversely proportional to the Reynolds number.

References

[1] N.K. Ghaddar, M. Magen, B.B. Mikic, A.T. Patera, Numerical investigation of incompressible flow in grooved channels. Part 2: resonance and oscillatory heat transfer enhancement, J. Fluid Mech. 168 (1986) 541–567.
[2] M. Greiner, An experimental investigation of resonant heat transfer heat transfer enhancement in grooved channels, Int. J. Heat Mass Transfer 34 (1991) 1383–1391.
[3] M.R. Mackley, P. Stonstreet, Heat transfer associated energy dissipation for oscillatory flow in baffled tubes, Chem. Eng. Sci. 50 (1995) 2211–2224.
[4] S.Y. Kim, B.H. Kang, J.M. Hyun, Forced convection heat transfer from two heated blocks in pulsating channel flow, Int. J. Heat Mass Transfer 41 (1998) 625–634.
[5] J.W. Moon, S.Y. Kim, H.H. Cho, Frequency-dependent heat transfer enhancement from rectangular heated block array in a pulsating channel flow, Int. J. Heat Mass Transfer 41 (2005) 625–634.
[6] T. Nishimura, N. Oka, Y. Yoshinaka, K. Kunitsugu, Influence of imposed oscillatory on the mass transfer enhancement of grooved channels for pulsatile flow, Int. J. Heat Mass Transfer 43 (2000) 4904–4913.
[7] T. Nishimura, N. Kojima, Mass transfer enhancement in a symmetric sinusoidal wavy-walled channel for pulsatile flow, Int. J. Heat Mass Transfer 38 (1995) 1719–1731.
[8] T. Nishimura, S. Matsune, Vortices and wall shear stresses in asymmetric and symmetric channels with sinusoidal wavy walls for pulsatile flow at low Reynolds numbers, Int. J. Heat Fluid Flow 9 (1998) 583–593.
[9] B.Y. Lee, I.S. Kang, H.C. Lim, Chaotic mixing and mass transfer enhancement by pulsatile flow in an axisymetric wavy channel, Int. J. Heat Mass Transfer 42 (1999) 2571–2581.
[10] J.A.W. Gut, J.M. Pinto, Modeling of plate heat exchangers with generalized configurations, Int. J. Heat Mass Transfer 46 (2003) 2571–2585.
[11] M. Greiner, R.F. Chen, R.A. Wirtz, Heat transfer augmentation through wall-shape-induced flow destabilization, J. Heat Transfer 112 (1990) 336–341.
[12] F.M. White, Viscous Fluid Flow, McGraw-Hill, Boston, 1974.
[13] G. Russ, H. Beer, Heat transfer and flow field in a pipe with sinusoidal wavy surface. II Experimental investigation, Int. J. Heat Mass Transfer 40 (1997) 1071–1081.
[14] M. Greiner, P.F. Fischer, H. Tufo, Numerical simulations of resonant heat transfer augmentation at low Reynolds numbers, J. Heat Transfer 124 (2002) 1169–1175.